

## Modeling Stellar Ca II H and K Emission Variations: Spot Contribution to the *S*-index.

K. SOWMYA,<sup>1</sup> A. I. SHAPIRO,<sup>1</sup> L. H. M. ROUPPE VAN DER VOORT,<sup>2,3</sup> N. A. KRIVOVA,<sup>1</sup> AND S. K. SOLANKI<sup>1</sup>

<sup>1</sup>*Max-Planck-Institut für Sonnensystemforschung, Justus-von-Liebig-Weg 3, 37077 Göttingen, Germany*

<sup>2</sup>*Institute of Theoretical Astrophysics, University of Oslo, PO Box 1029, Blindern 0315 Oslo, Norway*

<sup>3</sup>*Roseland Centre for Solar Physics, University of Oslo, PO Box 1029, Blindern 0315 Oslo, Norway*

(Received September 13, 2023)

Submitted to ApJL

### ABSTRACT

The *S*-index is a measure of emission in the Ca II H and K lines and is a widely used proxy of stellar magnetic activity. It has been assumed until now that the *S*-index is mainly affected by bright plage regions in the chromosphere. In particular, the effect of starspots on the *S*-index has been neglected. In this study we revisit this assumption. For this we analyze high-resolution observations of sunspots recorded in the Ca II H spectral line at the Swedish 1-m Solar Telescope and determine the contrast of spots with respect to the quiet surroundings. We find that the Ca II H line core averaged over whole sunspots (including superpenumbrae) is brighter than in the quiet surroundings and that the spot contrast in the line core is comparable to the facular contrast. This allows us to get a first estimate of the influence of spots on the *S*-index. We show that spots increase the *S*-index. While this increase is quite small for the Sun, it becomes significantly larger for more active stars. Further, we show that the inclusion of the contribution of spots to the *S*-index strongly affects the relationship between the *S*-index and stellar disk area coverages by spots and faculae, and present the new relations.

*Keywords:* Stellar activity – Stellar chromospheres – Starspots – Sunspots – Plages

### 1. INTRODUCTION

Concentrated magnetic fields on the photospheres of late-type stars form dark spots and bright faculae. Such magnetic fields extend to the chromosphere where they cause additional non-thermal heating and lead to the formation of chromospheric magnetic features. One of the most exciting manifestations of appearance and disappearance of magnetic features on the visible stellar surface (either due to their evolution or due to the stellar rotation) is variations of stellar brightness. Namely, the photospheric features cause variations observed in broadband photometric passbands, while the chromospheric features are responsible for variability in strong spectral lines like Ca II H and K which are amongst the most widely used proxy for stellar magnetic activity (see, e.g., Hall 2008, and references therein).

Brightness variations are very well studied for the Sun (Solanki et al. 2013; Ermolli et al. 2013). In the visible and infrared spectral domains they are affected by the interplay of photospheric spots and faculae (Solanki et al. 2013; Shapiro et al. 2016). At the same time the variability of the solar Ca II H and K emission is mainly driven by plages, which are the chromospheric counterpart of faculae (so that the same concentration of magnetic fields causes faculae in the photosphere and plages in the chromosphere). The spot contribution to solar Ca II H and K variability is believed to be small (Shapiro et al. 2014; Sowmya et al. 2021, hereafter Paper I) because plages are very bright in Ca II H and K lines (e.g. see Figure 1 of Skumanich et al. 1984) and on the Sun their area coverages are significantly larger than that of spots. As a result solar Ca II H and K emission is even often considered as a proxy of facular contribution to solar

irradiance variability (Lean 2000; Walton et al. 2003; Chapman et al. 2013; Berrilli et al. 2020). However, the role of spots in Ca II H and K variability of other stars has not been investigated before.

Stellar Ca II H and K emission measurements date back to Mount Wilson Observatory’s HK project in the 1960s which led to the establishment of the well known chromospheric activity indicator called the  $S$ -index (Vaughan et al. 1978), which is proportional to the summed fluxes in the H and K passbands covering the cores of the Ca II H and K lines, normalized to the summed fluxes in the nearby pseudo-continuum R and V passbands (see Paper I, for the definition of the passbands and  $S$ -index). The HK project was followed by Lowell observatory’s monitoring of the chromospheric activity simultaneously with photometric brightness (Lockwood et al. 1992). A combination of the data from this survey and the HK project revealed that old and less active stars like the Sun showed a direct correlation between the photometric brightness and the chromospheric activity while young active stars showed an anti-correlation (Lockwood et al. 1992, 2007; Radick et al. 1998, 2018), indicating a transition from faculae-dominated to spot-dominated brightness variability. This observed transition was explained to be due to surface coverages of spots growing much faster with activity than that of faculae (Foukal 1993; Chapman et al. 1997; Foukal 1998; Shapiro et al. 2014; Nèmec et al. 2022). Thus, for more active stars, spots are expected to have a stronger contribution to the  $S$ -index variability, prompting a quantitative assessment of their effect.

The main hurdle in assessing the impact of spots on stellar  $S$ -index values is the absence of any reliable information on spot chromospheres. Since direct observations of starspots in Ca II H and K lines are not yet feasible the most straightforward way to circumvent this hurdle is to utilize solar observations. Such observations have very recently become available thanks to the CHROMospheric Imaging Spectrometer (CHROMIS) on the Swedish 1-m Solar Telescope (SST; Scharmer et al. 2003) which observes the Sun with unprecedented spatial and good spectral resolution. Here we analyze the SST data of three sunspots in the Ca II H line at 3968.47 Å to determine the brightness of chromospheric counterparts of spots. The details of the data analysis and modelling approach are given in Section 2. Making use of the observed sunspot contrast, we evaluate the spot contribution to the  $S$ -index values of the Sun and active Sun-like stars. We present our findings in Section 3 and conclusions in Section 4.

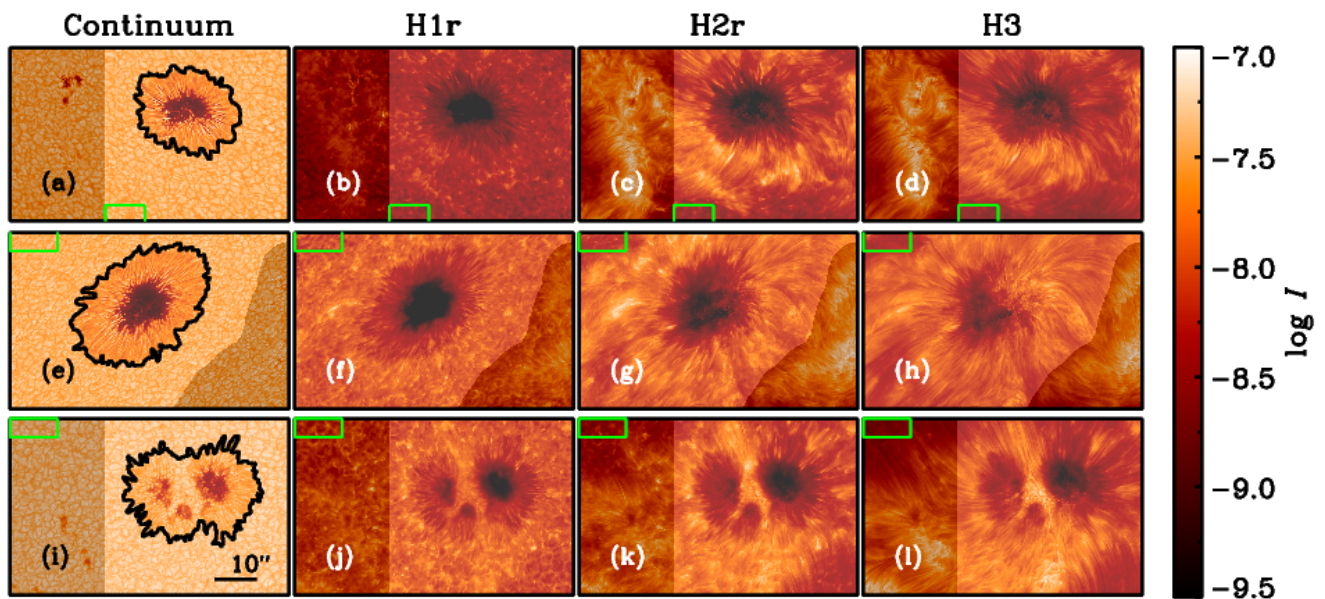


**Figure 1.** Intensity images of the three sunspots scanned on 07-08-2020 at  $\mu = 0.83$  (top row), on 22-06-2021 at  $\mu = 0.63$  (middle row), and on 07-07-2022 at  $\mu = 0.96$  (bottom row). The images cover an angular area of roughly  $67'' \times 42''$ . The sunspots are shown in the continuum at  $\sim 4001 \text{ \AA}$  (first column), and at wavelengths corresponding to H1r (second column), H2r (third column) and H3 (fourth column) as marked in Figure 2. The regions shown with lower transparency mask the areas contaminated by bright facular and plage patches. These regions are excluded from the analysis. Green boxes in each panel indicate the patches used for calculating the quiet Sun intensity profiles shown in Figure 2. Black contours in the first column mark the boundary of the sunspot. See text for details.

## 2. METHODS

### 2.1. Modeling stellar chromospheric activity

In [Paper I](#), we modeled the  $S$ -index for stars with solar activity level by neglecting spots since their surface coverages are much smaller than those of faculae. Spots were assumed to affect the fluxes in the H and K as well as R and V passbands in the same way so that their effect would vanish when the flux ratio is taken. Here, the goal is to determine the  $S$ -index by including the actually observed properties of spots and investigate what effect spots have on the  $S$ -index of the Sun and other, more active, stars. Therefore, in our current approach to synthesize the  $S$ -index, the total flux from the stellar disk at time  $t$  in each of the four passbands is computed by combining the contributions from the quiet star with that from spots and faculae. The stellar disk is split into  $l$  rings and the flux values calculated in these rings are summed up to obtain the total flux from the disk. Our approach can be summarised through the following equation for the total flux  $N_m(t)$ :

$$\begin{aligned}
 N_m(t) = & \sum_l \left[ \int_m I^q(\lambda_m, \mu_l) \text{Tr}(m) d\lambda \right] \Delta\Omega_l \\
 & + \sum_l \alpha_l^f(t) \left[ \int_m (I^f(\lambda_m, \mu_l) - I^q(\lambda_m, \mu_l)) \text{Tr}(m) d\lambda \right] \Delta\Omega_l \\
 & + \sum_l \alpha_l^s(t) \left[ \int_m (I^s(\lambda_m, \mu_l) - I^q(\lambda_m, \mu_l)) \text{Tr}(m) d\lambda \right] \Delta\Omega_l,
 \end{aligned} \tag{1}$$

with ‘m’ representing H, K, R, and V passbands.  $\alpha_l^f$  and  $\alpha_l^s$  are the time-dependent disk area coverages of faculae and spots in a ring at a limb distance of  $\mu_l$  which subtends a solid angle  $\Delta\Omega_l$ .  $I$  are the intensities from a given feature that depend on wavelength,  $\lambda_m$ , and  $\mu_l$ .  $\text{Tr}(m)$  are the transmission profiles of the H, K, R, and V passbands.

The quiet star flux (first term in Equation (1)) is determined using spectra synthesized from the standard 1D semi-empirical model C of [Fontenla et al. \(1999\)](#) while facular and plage fluxes (second term in Equation (1)) are obtained using spectra from model P of [Fontenla et al. \(1999\)](#). As explained in [Paper I](#), magnetic flux concentrations forming faculae on the photosphere undergo expansion in the chromosphere where they form plages. Due to this expansion, chromospheric plages cover larger areas on the Sun as compared to the photospheric faculae. In order to account for this expansion, we multiply faculae coverages  $\alpha_l^f$  by a constant expansion factor while computing plage spectral fluxes. Essentially, the plage area coverages are taken to be 2.9 times the faculae area coverages. This value is slightly smaller than 3.2 used in [Paper I](#) due to a number of minor adjustments in the model. Further details on the spectral synthesis and the use of a constant expansion factor are given in [Paper I](#).

We take the following approach for computing the spot contribution (last term in Equation (1)) to the total disk-integrated flux. For the pseudo-continuum R and V fluxes, we utilize spectra representing the photospheres of umbral and penumbral regions within spots computed by [Unruh et al. \(1999\)](#). These spectra have been well tested against available solar irradiance measurements ([Solanki et al. 2013](#); [Ermolli et al. 2013](#)). The chromosphere above sunspots is either missing or not very well represented in the existing 1D models of umbra and penumbra (see e.g. [Loukitcheva et al. 2017](#)). Therefore these models cannot be used to reliably determine the H and K fluxes of spots. Fortunately, in recent years, SST has observed sunspots in the Ca II spectral region with unprecedented spatial and good spectral resolution which makes it possible to study the chromospheric counterparts of spots in this spectral range. In the next section we detail these data and their analysis.

### 2.2. Determining spot brightness in H and K passbands

We analyse observations of sunspots in active regions (AR) AR12770, AR12833, and AR13046 obtained on 07-08-2020, 22-06-2021, and 07-07-2022, respectively, with CHROMIS at SST. CHROMIS is a dual Fabry-Pérot filtergraph system which carries out fast wavelength sampling of spectral lines. The spectral bandwidth FWHM of CHROMIS is about 120 mÅ. The imaging observations of the sunspot in AR12770 ( $\mu = \cos \theta = 0.83$ , with  $\theta$  being the heliocentric angle) were taken with 29 spectral points in the H line with a step size of 120 mÅ, including the central H3 absorption feature along with the blue(b)-red(r) H1 and H2 peaks. The spectral sampling was finer for the spots in AR12833 ( $\mu = 0.63$ ) and AR13046 ( $\mu = 0.96$ ), with 47 wavelength points separated by 60 mÅ in most parts of the H line. All three spots were also scanned in the continuum around 4001 Å. The CHROMIS angular pixel scale is 0.038". The

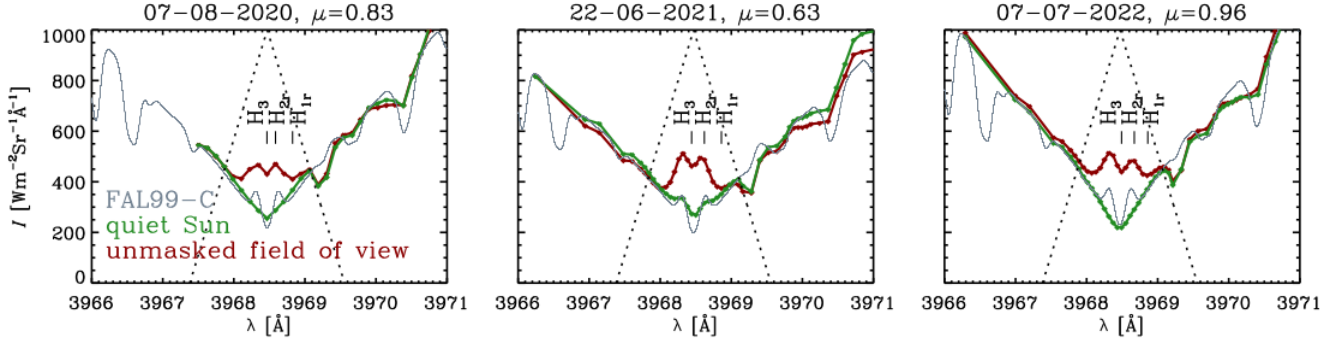


**Figure 2.** Average intensity profiles from the unmasked field of view in Figure 1 (maroon) and from the quiet Sun region marked by the green box in Figure 1 (green). Intensity profiles computed using the FAL99-C model of solar atmosphere (gray) are plotted for reference. The transmission profile of the H passband is shown by the dotted triangle. The H1r, H2r and H3 features are also marked.

observations cover a field of view of approximately  $67'' \times 42''$  and the duration of the spectral scan is between 10–15 seconds. The data were reduced following the CHROMISRED/SSTRED procedure outlined in Löfdahl et al. (2021).

Figure 1 shows observed images of the three spots at selected wavelengths. At chromospheric heights, the superpenumbrae of the spots become clearly visible (e.g. columns three and four). These superpenumbrae cover much larger areas than the spots at the photosphere. These superpenumbral regions are much brighter than the surrounding quiet regions (shown by green boxes in Figure 1). A visual inspection of the Ca II H far wing intensity images showed very bright facular patches lying close to the sunspot in the observed field of view (e.g. bright features on the left in Figure 1d). We mask these facular patches as shown in Figure 1, and exclude them from the analysis. In each sunspot scan, we identify the quiet regions in the field of view (shown by green boxes in Figure 1) and compute average intensity profiles,  $\langle I \rangle_{\text{qs}}$ , from within these regions. These profiles are plotted in green in Figure 2. We utilize spectra synthesized with the FAL99-C model to calibrate the observed quiet Sun profiles and determine the calibration factor. This factor is used to calibrate the entire image. We note that synthetic spectra computed with the FAL99-C model have been demonstrated to agree with FTS spectral atlas data (Neckel 1999; Doerr et al. 2016). We refer to Paper I for details.

Next we compute the average profile,  $\langle I \rangle_{\text{ufov}}$ , from the unmasked field of view (ufov) shown in Figure 1. The flux excess/deficit from the spot in the H passband is then calculated following

$$P_{\text{ufov}} = \int_{\text{H}} [\langle I \rangle_{\text{ufov}} \cdot N_{\text{ufov}}] d\Omega \text{Tr}(\text{H}) d\lambda, \quad (2)$$

$$P_{\text{qs}} = \int_{\text{H}} [\langle I \rangle_{\text{qs}} \cdot N_{\text{ufov}}] d\Omega \text{Tr}(\text{H}) d\lambda, \quad (3)$$

$$\Delta_{\text{spot}} = P_{\text{ufov}} - P_{\text{qs}}. \quad (4)$$

Here  $N_{\text{ufov}}$  is the total number of pixels within the unmasked field of view and  $d\Omega$  is the solid angle subtended by a pixel.  $P_{\text{ufov}}$  is the flux from the unmasked field of view which contains both spot and quiet regions.  $P_{\text{qs}}$  is the flux which would be measured if the entire unmasked field of view were covered by the quiet Sun. When the difference between these fluxes is calculated in Equation (4) the contribution of pixels corresponding to the quiet Sun gets cancelled out. Thus, what remains is the flux excess/deficit due to the spot, including the canopy.

The flux difference due to spots in  $\text{W m}^{-2}$  units calculated using Equation (4) is given in the fourth column of Table 1. The positive flux difference values indicate that the chromospheric counterparts of spots are brighter than the quiet surroundings, which is already clear from Figure 2 where the mean profiles from the unmasked field of view are much brighter in the line core compared to the mean quiet Sun profiles (compare maroon and green profiles). These flux values depend on the size of the sunspot. In order to remove this dependency, we divide the flux values by the projected sunspot area on the photosphere, i.e., the area enclosed within the black contours in Figure 1. The fifth column of Table 1 provides these area normalised fluxes. For comparison, the facular fluxes per unit area from Paper I are also given in Table 1. While somewhat lower, the sunspot brightness in H passband is still of comparable magnitude to the facular brightness.



**Table 1.** Spot brightness in H passband in comparison to the surrounding quiet Sun regions, calculated directly from SST data. The model values from Paper I for faculae are shown in the last column for reference.

DD-MM-YYYY	Active region	$\mu$	$\Delta_{\text{spot}} (\text{W m}^{-2})$	$\frac{\Delta_{\text{spot}} (\text{W m}^{-2})}{\text{spot area (km}^2)}$	$\frac{\Delta_{\text{faculae}} (\text{W m}^{-2})}{\text{faculae area (km}^2)}$
07-08-2020	12770	0.83	3.93e-06	1.94e-14	6.53e-14
22-06-2021	12833	0.63	4.56e-06	1.32e-14	6.38e-14
07-07-2022	13046	0.96	5.80e-06	2.04e-14	6.62e-14

CHROMIS observations analyzed in this study cover  $\mu$ -values from 0.96 down to 0.63 which corresponds to more than 50% of the solar disk. Nevertheless, to compute the spot contribution to the total disk-integrated flux in the H passband, we require spot contrasts outside the  $\mu$ -range covered by these observations. To obtain them, we make several experiments assuming various dependence of spot contrast on  $\mu$ . First, we make use of the centre to limb variation (CLV) of quiet Sun flux in the H passband calculated using the FAL99-C spectra. Earlier studies have shown that the Ca II H and K emission from the quiet Sun and faculae have the same CLV (e.g. Skumanich et al. 1984; Ermolli et al. 2007, 2010). Following this, we assume that the Ca II H and K emission from spots also has the same CLV as the quiet Sun. Then we use  $\mu = 0.84$  or  $\mu = 0.63$  observations to define the range of CLV dependences of spot contrast considered for  $S$ -index calculations (see grey shaded area in Figure 3). We also perform a linear regression fit to the observed data points which results in a much steeper CLV as shown by the blue line in Figure 3. Despite such a wide range of considered CLV dependences the resulting  $S$ -index values are very similar (see Section 3.2) so that the exact behaviour of the spot contrast outside the observed  $\mu$ -range has very little impact on the results of this study.

Further, we expect the flux difference due to spots in the K passband to be similar to that in the H passband. This is because the Ca II H and K lines have similar excitation energies and Einstein coefficients so that they form at nearly the same heights in the solar atmosphere and also respond similarly to the changes in the atmospheric structure associated with magnetic activity (e.g. Uitenbroek 1990). Therefore we use the CLV curves shown in Figure 3 also for the K passband. Furthermore, small sunspots with relatively simple morphologies similar to the ones shown in Figure 1 are found to be a lot more common than big sunspots (Bogdan et al. 1988; Baumann & Solanki 2005) that can have a more complex morphology. Hence, we expect that the morphology of sunspots shown in Figure 1 is representative of a good fraction of sunspots. Consequently, we use the same CLV for spots of all shapes and sizes.

### 3. INFLUENCE OF SPOTS ON THE $S$ -INDEX

We now compute the  $S$ -index using the method described in Section 2.1. First, we revisit the assumption made in Paper I that spot contribution to the solar  $S$ -index is negligible. Then we consider active stars with larger spot coverages than the Sun and evaluate, for the first time, how the  $S$ -index is affected by spots.

#### 3.1. The Sun

Figure 4 shows how sunspots influence the observed solar Ca II H and K emission. A comparison of the daily  $S$ -index timeseries for four solar activity cycles computed by including the contribution from spots and neglecting it is shown in Figures 4a-b, while Figures 4c-d show the 81-day smoothed values. We only present the calculations done using the CLV corresponding to the upper envelope of the grey region shown in Figure 3. This is because the solar  $S$ -index values computed for the range of CLVs shown in Figure 3 do not differ much. The area coverages of faculae and spots needed for the  $S$ -index computations are taken from Yeo et al. (2014), see Paper I for details.

Sunspots are dark in the photosphere compared to the quiet Sun so that they decrease solar flux in the R and V passbands. At the same time, the chromospheric counterparts of spots are brighter than the surrounding quiet regions so that spots enhance the total flux in the H and K passbands. Both of these effects lead to an increase of the  $S$ -index when sunspots are included in the calculations. The contribution of spots to  $S$ -index is, unsurprisingly, zero at minima of solar activity and increases towards activity maxima. Figure 4b shows that transits of large spot groups over the visible solar disk cause short-term increases of the  $S$ -index by up to 25% of the amplitude of the solar cycle 23 in  $S$ -index. At the same time Figure 4d shows that the effect of spots on 81-day smoothed values is significantly less and is below 7% of the amplitude of the solar cycle 23 in  $S$ -index.

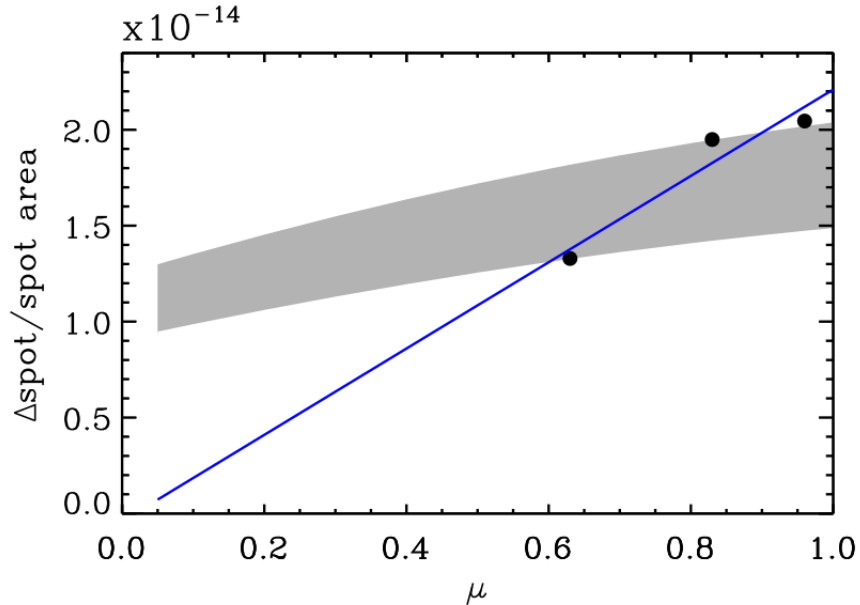


**Figure 3.** Center to limb variation of the flux excess due to spots. Black circles are the SST observations (values from fifth column of Table 1). Grey shaded region shows different scalings of the quiet Sun CLV to match observations. Blue line is the linear fit to the observed data points. See text for details.

All in all, since disk area coverages of solar faculae are much larger than those of spots and since faculae are a bit brighter than spots in the H and K passbands (see Table 1), the variations of the solar  $S$ -index are almost fully brought about by faculae with exceptions of periods when large sunspot groups transit the visible solar disk.

### 3.2. Active stars

A number of studies have shown that solar spot coverages increase with solar activity faster than those of faculae (e.g. Foukal 1993; Chapman et al. 1997; Foukal 1998; Yeo et al. 2021; Chatzistergos et al. 2022). Shapiro et al. (2014) and Nèmec et al. (2022) showed that the solar relation between facular and spot coverages can be extrapolated towards stars more active than the Sun. This implies that the ratio of spot-to-facular coverages is higher for active stars and, thus, the relative contribution of spots to their  $S$ -index values is expected to be higher than that reported for the Sun in Section 3.1.

To find the spot contribution to  $S$ -index of active stars we use the relationship between the spot and facular area coverages established based on the solar data (Shapiro et al. 2014; Nèmec 2021):

$$\alpha^f = a\sqrt{\alpha^s - b} + c, \quad (5)$$

where  $a, b, c$  are constants. Their values are 0.67,  $-0.0003$ , and  $-0.009$ , respectively. Here we assume that this relationship holds also for more active stars (see detailed discussion in Nèmec et al. 2022) and consider a series of spot area coverage values from 0 to 50%. Then we use Equation (5) to get the corresponding facular area coverages. The facular area coverages obtained in this way are shown as a function of spot area coverages in Figure 5a. For simplicity, we assume that spots and faculae are uniformly distributed on the stellar disk and use the model described in Section 2 to calculate  $S$ -index values.

Figure 5b shows the  $S$ -index values calculated by including both faculae and spots plotted as a function of  $S$ -index values computed by completely neglecting spots (or rather assuming that they are equally dark in Ca II H and K line cores and continuum as was done in Paper I). The blue curve and the grey shaded area represent the cases when the spot contribution is taken into account both in the line cores (H and K) and in the continuum (R and V). For the line cores, we use the entire range of CLVs shown in Figure 3 while for the continuum, we use the CLV computed using synthetic spectra from Unruh et al. (1999). We see from Figure 5b that different CLVs of the line core contrasts lead to very small changes in the  $S$ -index values, which is reassuring. It is also clear from this plot that the contribution from spots to  $S$ -index becomes progressively more significant with increasing spot coverages. Spots lead to a steep

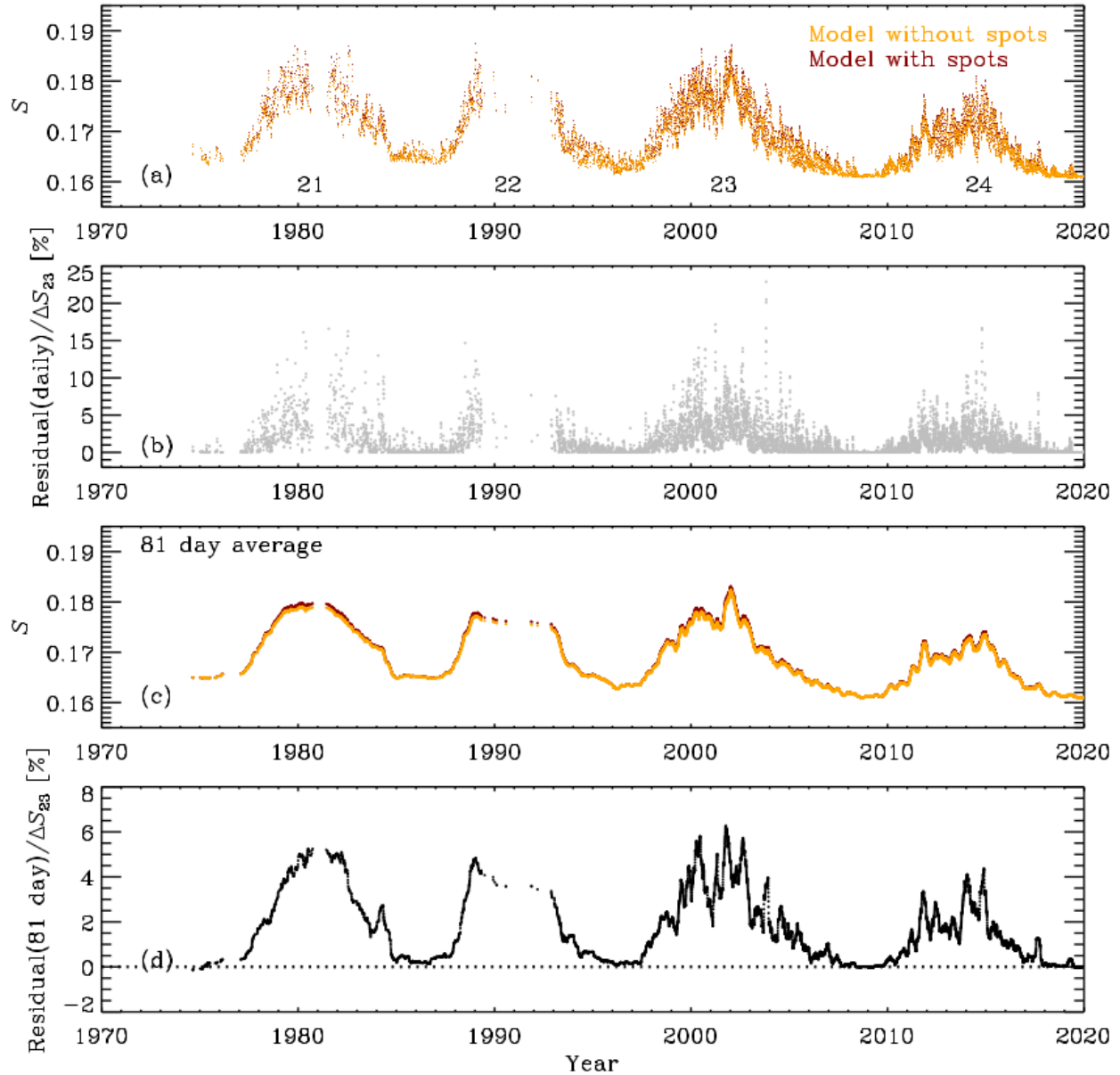


**Figure 4.** Panel a: comparison between the solar  $S$ -index values computed including (maroon) and excluding (orange) the contribution from spots. Panel b: difference between the daily  $S$ -index values shown in panel (a) normalised to the amplitude of the solar cycle 23 in  $S$ -index, which is 0.0149. Panel c: 81 day smoothed values of the  $S$ -index time series plotted in panel (a). Panel d: difference between the 81 day averaged values shown in panel (c) normalised to the amplitude of the solar cycle 23 in  $S$ -index.

increase of the  $S$ -index by decreasing the radiative flux in the continuum and increasing it in the Ca II H and K line cores.

Further, we do an experiment to understand which of the two effects from spots, namely the reduction in the continuum flux and enhancement of the line core flux, is the dominant one. In this experiment the chromospheric counterparts of spots are assumed to be as bright as the quiet chromosphere so that they do not affect the line core flux. However, the effect of spots on the continuum flux is still accounted for. The resulting  $S$ -index values from this experiment are shown by the salmon curve in Figure 5b. A comparison of the salmon curve with the other cases shown in Figure 5b suggests that the effect arising from the decrease of continuum fluxes is slightly larger than that from the

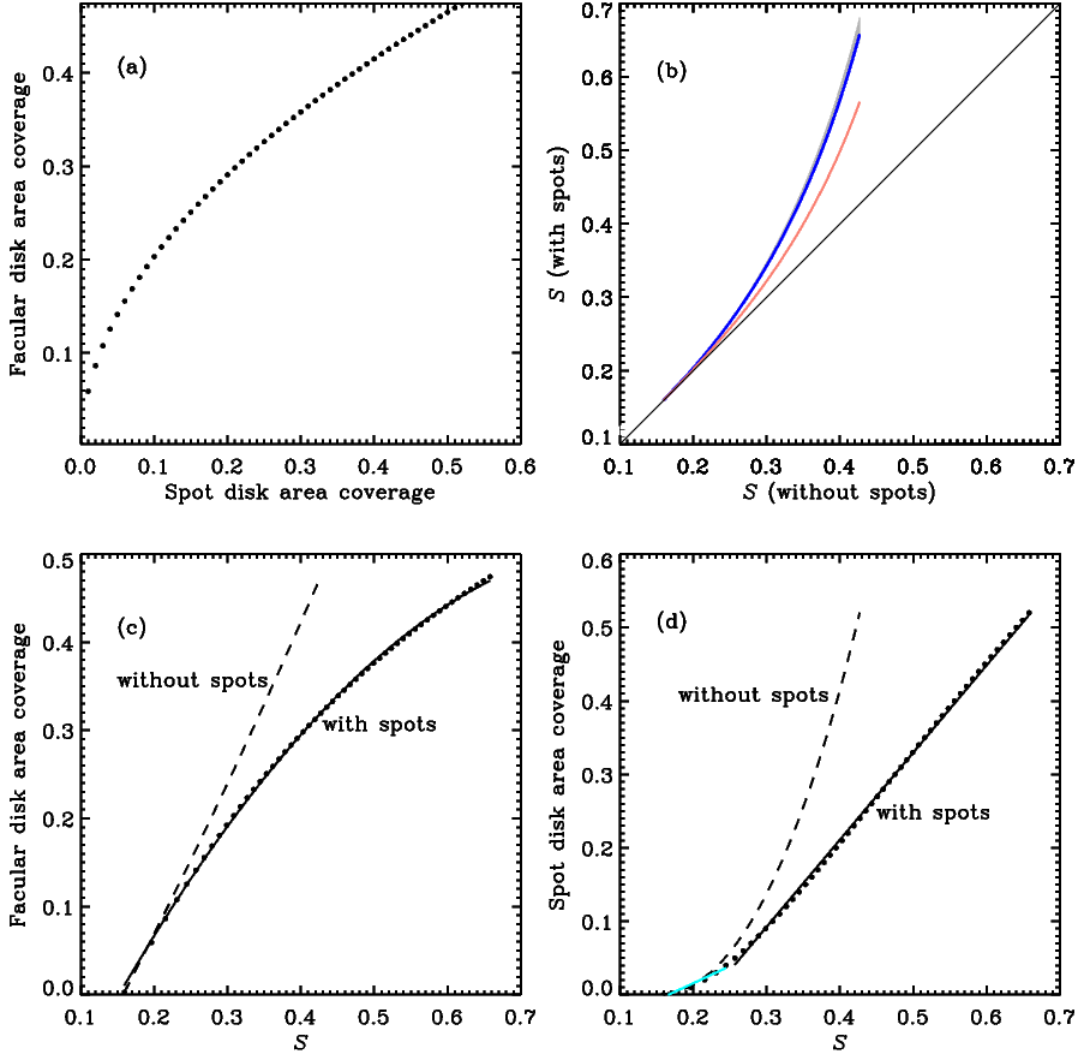


**Figure 5.** Panel a: photospheric disk area coverages of faculae as a function of the corresponding spot area coverages, see text for details. Panel b:  $S$ -index with spots as a function of  $S$ -index without spots. The blue curve and the grey shaded area are obtained using the spot contrast CLVs shown in Figure 3. The salmon curve represents the case where we assume that spots are as bright as the quiet star in H and K so that they are invisible in the chromosphere but are still visible as dark features in the photosphere. The black line shows the case when spots are neglected completely. Panel c: relationship between facular area coverages and  $S$ -index with spots (filled circles) along with the quadratic fit to this relationship (solid line). The dashed line shows the dependence of facular disk area coverage on  $S$ -index without spots. Panel d: relationship between spot area coverages and  $S$ -index with spots (filled circles) along with the linear fits (cyan and black solid lines) to their relationship. The dashed line shows the dependence of spot disk area coverages on  $S$ -index without spots.

increase of the flux in the line core. All in all, the contribution of spots to the  $S$ -index cannot be neglected for active stars, e.g. the error in the  $S$ -index resulting from neglecting spots reaches 16% for  $S = 0.3$  and 30% for  $S = 0.35$ .

In Figures 5c-d, we show the relationship between the  $S$ -index computed with spots (representing the upper envelope of the grey shaded area in Figure 5b) and disk area coverages of spots and faculae. Facular disk area coverages show a quadratic dependence on the  $S$ -index while the spot disk area coverages increase linearly with the  $S$ -index. We find the following dependence for the faculae disk area coverages:

$$\alpha^f(S) = -0.246 + 1.773 S - 1.032 S^2, \quad (6)$$



and for the spot disk area coverages:

$$\alpha^s(S) = \begin{cases} -0.078 + 0.466S & \text{if } S < 0.25 ; \\ -0.269 + 1.209S & \text{if } S \geq 0.25 , \end{cases} \quad (7)$$

where  $S$  here is the  $S$ -index computed by including spots.

Figures 5c-d point to a linear relationship for faculae disk area coverages and quadratic relationship for spot disk area coverages as a function of  $S$ -index when spot contribution to the  $S$ -index is neglected. The same functional relationships (see their Eqs. 1–2) have been found by Shapiro et al. (2014) using solar data, i.e. in the regime when  $S$ -index variability is mainly driven by faculae. Our result shows that the spot contribution to the  $S$ -index for active stars changes the functional form of the dependence of the facular and spot disk area coverages on the  $S$ -index.

#### 4. SUMMARY AND DISCUSSION

While empirical and physics-based models attribute faculae/plage to be the main contributors to the  $S$ -index thereby neglecting spots, the role played by spots was until now poorly understood. In this paper, for the first time, we explored the effect of spots on stellar Ca II H and K emission. For this purpose, we used high quality observations of three sunspots from SST. The analysis of these sunspots revealed that in the Ca II H and K line cores, sunspots are brighter than the quiet Sun regions, thus leading to a positive contrast value in the H and K passbands. The sunspots are nearly as bright as faculae in these spectral passbands. Spots reduce the total flux in the R and V passbands because they are dark in the photosphere while at the same time they increase the total H and K flux. Together, the two effects lead to an enhancement in the  $S$ -index.

For an old, less-active star like the Sun, disk area coverages of spots are significantly smaller than those of faculae. Because of this, the increase in the  $S$ -index caused by sunspots is only a small fraction of the observed solar  $S$ -index and its variability. Therefore, we confirm that neglecting the spot contribution is a reasonable choice when modeling the  $S$ -index of inactive stars like the Sun. However, we find that spots have a great impact on the  $S$ -index for young and active stars. Thus, spot contribution cannot be neglected when interpreting measurements of the  $S$ -index and its variability in active stars. We also find, under the assumptions of the modelling approach we used, that for active stars the facular disk area coverages show a quadratic dependence on the  $S$ -index while the dependence for spot disk coverage is linear.

An important limitation of our modeling approach is that it does not allow accounting for the interaction between chromospheric counterparts of different active regions. Along the same line, chromospheric superpenumbrae of different spots within an active region can also interact with each other if the spots get packed too tightly. These effects are outside of the scope of this study and warrant further investigation.

Although metrics based on stellar photometric brightness have recently emerged as magnetic activity indicators (e.g. Basri et al. 2013), the  $S$ -index still serves as an important proxy for stellar activity. A plethora of  $S$ -index data has recently been collected by surveys targeting exoplanets. For example, the Keck and Lick observatories have recorded  $S$ -indices of over 2000 FGKM dwarfs as part of the California Planet Search program (Wright et al. 2004; Isaacson & Fischer 2010). The High Accuracy Radial velocity Planet Searcher (HARPS; Mayor et al. 2003) provides  $S$ -indices of over 1600 FGK stars (e.g. Gomes da Silva et al. 2021). Observations of the chromospheric emission from stars, including extended monitoring of those in the Mount Wilson HK sample, are expected from the EXtreme PREcision Spectrometer (EXPRES; Jurgenson et al. 2016) at Lowell observatory. Furthermore, the spectroscopic survey by the Large Sky Area Multi-Object Fibre Spectroscopic Telescope (LAMOST; Cui et al. 2012; Zhao et al. 2012) has allowed measuring chromospheric activity of hundreds of thousands of stars (Yan et al. 2022; Zhang et al. 2022). All these measurements show a considerable spread in the  $S$ -index distribution of stars belonging to a given spectral type. An understanding of the main drivers of the chromospheric activity of these stars will greatly benefit the interpretation of their  $S$ -index measurements.

Here we considered the effect of spots on Ca II H and K emission from stars with solar fundamental parameters. In the forthcoming publication we plan to study the effect of spots on activity cycles of stars using the surface flux transport simulations (Işık et al. 2018; Nèmec et al. 2023).

1 We thank the anonymous referee for their helpful comments. The Swedish 1-m Solar Telescope is operated on the  
 2 island of La Palma by the Institute for Solar Physics of Stockholm University in the Spanish Observatorio del Roque de  
 3 los Muchachos of the Instituto de Astrofísica de Canarias. The Institute for Solar Physics is supported by a grant for  
 4 research infrastructures of national importance from the Swedish Research Council (registration number 2021-00169).  
 5 LRvdV is supported by the Research Council of Norway, project number 325491, and through its Centres of Excellence  
 6 scheme, project number 262622. This study has made use of SAO/NASA Astrophysics Data System’s bibliographic  
 7 services.

## REFERENCES

- Basri, G., Walkowicz, L. M., & Reiners, A. 2013, *ApJ*, 769, 37, doi: [10.1088/0004-637X/769/1/37](https://doi.org/10.1088/0004-637X/769/1/37)
- Baumann, I., & Solanki, S. K. 2005, *A&A*, 443, 1061, doi: [10.1051/0004-6361:20053415](https://doi.org/10.1051/0004-6361:20053415)
- Berrilli, F., Criscuoli, S., Penza, V., & Lovric, M. 2020, *SoPh*, 295, 38, doi: [10.1007/s11207-020-01603-5](https://doi.org/10.1007/s11207-020-01603-5)
- Bogdan, T. J., Gilman, P. A., Lerche, I., & Howard, R. 1988, *ApJ*, 327, 451, doi: [10.1086/166206](https://doi.org/10.1086/166206)
- Chapman, G. A., Cookson, A. M., & Dobias, J. J. 1997, *ApJ*, 482, 541, doi: [10.1086/304138](https://doi.org/10.1086/304138)
- Chapman, G. A., Cookson, A. M., & Preminger, D. G. 2013, *SoPh*, 283, 295, doi: [10.1007/s11207-013-0233-8](https://doi.org/10.1007/s11207-013-0233-8)
- Chatzistergos, T., Ermolli, I., Krivova, N. A., et al. 2022, *A&A*, 667, A167, doi: [10.1051/0004-6361/202244913](https://doi.org/10.1051/0004-6361/202244913)
- Cui, X.-Q., Zhao, Y.-H., Chu, Y.-Q., et al. 2012, *Research in Astronomy and Astrophysics*, 12, 1197, doi: [10.1088/1674-4527/12/9/003](https://doi.org/10.1088/1674-4527/12/9/003)
- Doerr, H. P., Vitas, N., & Fabbian, D. 2016, *A&A*, 590, A118, doi: [10.1051/0004-6361/201628570](https://doi.org/10.1051/0004-6361/201628570)
- Ermolli, I., Criscuoli, S., Centrone, M., Giorgi, F., & Penza, V. 2007, *A&A*, 465, 305, doi: [10.1051/0004-6361:20065995](https://doi.org/10.1051/0004-6361:20065995)
- Ermolli, I., Criscuoli, S., Uitenbroek, H., et al. 2010, *A&A*, 523, A55, doi: [10.1051/0004-6361/201014762](https://doi.org/10.1051/0004-6361/201014762)
- Ermolli, I., Matthes, K., Dudok de Wit, T., et al. 2013, *Atmospheric Chemistry & Physics*, 13, 3945, doi: [10.5194/acp-13-3945-2013](https://doi.org/10.5194/acp-13-3945-2013)
- Fontenla, J., White, O. R., Fox, P. A., Avrett, E. H., & Kurucz, R. L. 1999, *ApJ*, 518, 480, doi: [10.1086/307258](https://doi.org/10.1086/307258)
- Foukal, P. 1993, *SoPh*, 148, 219, doi: [10.1007/BF00645087](https://doi.org/10.1007/BF00645087)
- . 1998, *ApJ*, 500, 958, doi: [10.1086/305764](https://doi.org/10.1086/305764)
- Gomes da Silva, J., Santos, N. C., Adibekyan, V., et al. 2021, *A&A*, 646, A77, doi: [10.1051/0004-6361/202039765](https://doi.org/10.1051/0004-6361/202039765)
- Hall, J. C. 2008, *Living Reviews in Solar Physics*, 5, 2, doi: [10.12942/lrsp-2008-2](https://doi.org/10.12942/lrsp-2008-2)
- Işık, E., Solanki, S. K., Krivova, N. A., & Shapiro, A. I. 2018, *A&A*, 620, A177, doi: [10.1051/0004-6361/201833393](https://doi.org/10.1051/0004-6361/201833393)
- Isaacson, H., & Fischer, D. 2010, *ApJ*, 725, 875, doi: [10.1088/0004-637X/725/1/875](https://doi.org/10.1088/0004-637X/725/1/875)
- Jurgenson, C., Fischer, D., McCracken, T., et al. 2016, in *Society of Photo-Optical Instrumentation Engineers (SPIE) Conference Series*, Vol. 9908, Ground-based and Airborne Instrumentation for Astronomy VI, ed. C. J. Evans, L. Simard, & H. Takami, 99086T, doi: [10.1117/12.2233002](https://doi.org/10.1117/12.2233002)
- Lean, J. 2000, *Geophys. Res. Lett.*, 27, 2425, doi: [10.1029/2000GL000043](https://doi.org/10.1029/2000GL000043)
- Lockwood, G. W., Skiff, B. A., Baliunas, S. L., & Radick, R. R. 1992, *Nature*, 360, 653, doi: [10.1038/360653a0](https://doi.org/10.1038/360653a0)
- Lockwood, G. W., Skiff, B. A., Henry, G. W., et al. 2007, *ApJS*, 171, 260, doi: [10.1086/516752](https://doi.org/10.1086/516752)
- Löfdahl, M. G., Hillberg, T., de la Cruz Rodríguez, J., et al. 2021, *A&A*, 653, A68, doi: [10.1051/0004-6361/202141326](https://doi.org/10.1051/0004-6361/202141326)
- Loukitcheva, M. A., Iwai, K., Solanki, S. K., White, S. M., & Shimojo, M. 2017, *ApJ*, 850, 35, doi: [10.3847/1538-4357/aa91cc](https://doi.org/10.3847/1538-4357/aa91cc)
- Mayor, M., Pepe, F., Queloz, D., et al. 2003, *The Messenger*, 114, 20
- Neckel, H. 1999, *SoPh*, 184, 421, doi: [10.1023/A:1017165208013](https://doi.org/10.1023/A:1017165208013)
- Nèmec, N.-E. 2021, *arXiv e-prints*, arXiv:2106.13183, doi: [10.48550/arXiv.2106.13183](https://doi.org/10.48550/arXiv.2106.13183)
- Nèmec, N. E., Shapiro, A. I., Işık, E., Solanki, S. K., & Reinhold, T. 2023, *A&A*, 672, A138, doi: [10.1051/0004-6361/202244412](https://doi.org/10.1051/0004-6361/202244412)
- Nèmec, N. E., Shapiro, A. I., Işık, E., et al. 2022, *ApJL*, 934, L23, doi: [10.3847/2041-8213/ac8155](https://doi.org/10.3847/2041-8213/ac8155)
- Radick, R. R., Lockwood, G. W., Henry, G. W., Hall, J. C., & Pevtsov, A. A. 2018, *ApJ*, 855, 75, doi: [10.3847/1538-4357/aaae3](https://doi.org/10.3847/1538-4357/aaae3)
- Radick, R. R., Lockwood, G. W., Skiff, B. A., & Baliunas, S. L. 1998, *ApJS*, 118, 239, doi: [10.1086/313135](https://doi.org/10.1086/313135)

- Scharmer, G. B., Bjelksjo, K., Korhonen, T. K., Lindberg, B., & Petterson, B. 2003, in *Society of Photo-Optical Instrumentation Engineers (SPIE) Conference Series*, Vol. 4853, *Innovative Telescopes and Instrumentation for Solar Astrophysics*, ed. S. L. Keil & S. V. Avakyan, 341–350, doi: [10.1117/12.460377](https://doi.org/10.1117/12.460377)
- Shapiro, A. I., Solanki, S. K., Krivova, N. A., et al. 2014, *A&A*, 569, A38, doi: [10.1051/0004-6361/201323086](https://doi.org/10.1051/0004-6361/201323086)
- Shapiro, A. I., Solanki, S. K., Krivova, N. A., Yeo, K. L., & Schmutz, W. K. 2016, *A&A*, 589, A46, doi: [10.1051/0004-6361/201527527](https://doi.org/10.1051/0004-6361/201527527)
- Skumanich, A., Lean, J. L., Livingston, W. C., & White, O. R. 1984, *ApJ*, 282, 776, doi: [10.1086/162262](https://doi.org/10.1086/162262)
- Solanki, S. K., Krivova, N. A., & Haigh, J. D. 2013, *ARA&A*, 51, 311, doi: [10.1146/annurev-astro-082812-141007](https://doi.org/10.1146/annurev-astro-082812-141007)
- Sowmya, K., Shapiro, A. I., Witzke, V., et al. 2021, *ApJ*, 914, 21, doi: [10.3847/1538-4357/abf247](https://doi.org/10.3847/1538-4357/abf247)
- Uitenbroek, H. 1990, PhD thesis, University of Utrecht, Netherlands
- Unruh, Y. C., Solanki, S. K., & Fligge, M. 1999, *A&A*, 345, 635
- Vaughan, A. H., Preston, G. W., & Wilson, O. C. 1978, *PASP*, 90, 267, doi: [10.1086/130324](https://doi.org/10.1086/130324)
- Walton, S. R., Preminger, D. G., & Chapman, G. A. 2003, *ApJ*, 590, 1088, doi: [10.1086/375022](https://doi.org/10.1086/375022)
- Wright, J. T., Marcy, G. W., Butler, R. P., & Vogt, S. S. 2004, *ApJS*, 152, 261, doi: [10.1086/386283](https://doi.org/10.1086/386283)
- Yan, H., Li, H., Wang, S., et al. 2022, *The Innovation*, 3, 100224, doi: [10.1016/j.xinn.2022.100224](https://doi.org/10.1016/j.xinn.2022.100224)
- Yeo, K. L., Krivova, N. A., Solanki, S. K., & Glassmeier, K. H. 2014, *A&A*, 570, A85, doi: [10.1051/0004-6361/201423628](https://doi.org/10.1051/0004-6361/201423628)
- Yeo, K. L., Solanki, S. K., Krivova, N. A., & Jiang, J. 2021, *A&A*, 654, A28, doi: [10.1051/0004-6361/202141336](https://doi.org/10.1051/0004-6361/202141336)
- Zhang, W., Zhang, J., He, H., et al. 2022, *ApJS*, 263, 12, doi: [10.3847/1538-4365/ac9406](https://doi.org/10.3847/1538-4365/ac9406)
- Zhao, G., Zhao, Y.-H., Chu, Y.-Q., Jing, Y.-P., & Deng, L.-C. 2012, *Research in Astronomy and Astrophysics*, 12, 723, doi: [10.1088/1674-4527/12/7/002](https://doi.org/10.1088/1674-4527/12/7/002)